Steric and Kinetic Isotope Effects in the Deprotonation of Cation Radicals of NADH Synthetic Analogues

Agnès Anne, Sylvie Fraoua, Philippe Hapiot, Jacques Moiroux,* and Jean-Michel Savéant*

Contribution from the Laboratoire d'Electrochimie Moléculaire de l'Université Denis Diderot (Paris 7), 2 place Jussieu, 75251 Paris, Cedex 05, France

Received February 27, 1995[⊗]

Abstract: The deprotonation rate constants and kinetic isotope effects of the cation radicals have been determined by combined use of direct electrochemical techniques at micro- and ultramicroelectrodes, redox catalysis, and laser flash photolysis, over a extended series of opposing bases. Significant steric hindrance to deprotonation results from encumbering of the opposing base and of the functional carbon in the cation radical by alkyl groups. Kinetic isotope effects, ranging from 2 to 12 in terms of k_H/k_D, appear upon substituting H to D at the functional carbon of the cation radical. The modest magnitude of the kinetic isotope effects and the fact that they are insensitive to steric hindrance show that proton (or H-atom) tunneling does not interfere significantly in the deprotonation reaction. All the cation radicals in the methylacridan series are strong acids, with pK_a's ranging from 0.8 to 1.7, as determined from thermodynamic cycles involving measured standard potentials and hydride-transfer equilibrium constants.

Cation radicals are generally much stronger carbon acids than the molecules from which they derive by electrochemical or homogeneous oxidation. Thus, besides the rather restricted set of molecules where the acidity of hydrogens borne by a carbon atom is enhanced by the proximity of a strongly electron-withdrawing substituent,[1] a large family of additional carbon acids is made available for studying the dynamics of proton transfer. Together with the importance of cation radical intermediates in the oxidation of organic molecules, this is one reason for the continuous and active attention that is being paid to deprotonation of cation radicals.[2] Among these, cation radicals deriving from NADH analogues offer the additional interest that a good understanding of the dynamics of their deprotonation[3,4] is important in the discussion of the mechanism of formal hydride transfers (true hydride transfers or $H^+ + 2e^-$ transfers?) involving NADH itself or its synthetic analogues.[5]

Previous studies of deprotonation of NADH analogue cation radicals ($BNAH_2$, $BQAH_2$, $BQCNH_2$, and $N(CH_3)MAH_2$ in Chart 1) by an extended series of bases (pyridines, amines, and carboxylates) spanning 18 pK_a units revealed a good correlation between the deprotonation rate constants, k, and ΔpK_a independently from the nature of the opposing base.[3] From the smallest measurable rate constant up to the diffusion limit, the log $k - \Delta pK_a$ plots could be fitted with quadratic activation/driving force equations showing consistency between the magnitude of the intrinsic barrier and the average value of the symmetry factor. It was noticed that the intrinsic barrier correlates with the homolytic bond C−H bond dissociation energy in the cation radical as predicted by dissociative electron-transfer theory,[6] thus pointing to the concept that deprotonation in this case is best represented by a concerted electron−H-atom transfer rather than a *stricto sensu* proton transfer.

These studies purposely avoided the presence of sterically encumbering substituents on the opposing base, such as alkyl groups in the 2 or 2,6 positions of pyridines. One of the aims of the work described below was precisely to address the possibility of steric hindrance to deprotonation in the same series of cation radicals. In this connection, attention was focused on the reaction of the cation radicals of $BNAH_2$ and $N(CH_3)MAH_2$ (Chart 1) with pyridines bearing methyl substituents in the 2 and 6 positions. Another manner of studying steric hindrance to deprotonation was to encumber the functional carbon by alkyl or aryl groups as in $N(CH_3)MAHCH_3$, $N(CH_3)MAHCH_2Ph$ and $N(CH_3)MAHPh$ (Chart 1) and investigate the reaction of their cation radicals with unencumbered or encumbered bases.

Another aspect of the dynamics of deprotonation of NADH analogues cation radicals that has received little attention so far is kinetic isotope effects.[7] As described below, we have investigated such effects in the series of deuterated compounds shown in Chart 1. In order to uncover whether kinetic isotope effects in this family of acids provide unambiguous evidence for proton (or H-atom) tunneling,[8] we combined investigation of steric and isotope kinetic effects.

With non-radical carbon acids, such as nitro-substituted derivatives, large kinetic isotope effects have been observed and

[⊗] Abstract published in *Advance ACS Abstracts*, July 1, 1995.

(1) (a) Bell, R. P.; Goodall, D. M. *Proc. R. Soc. London, Ser. A* **1966**, *294*, 273. (b) Bordwell, F. G.; Boyle, W. J. *J. Am. Chem. Soc.* **1975**, *97*, 3447. (c) Bordwell, F. G.; Bartmess, J. E.; Hautalla, J. A. *J. Org Chem.* **1978**, *43*, 3107. Albery, W. J.; Campbell-Crawford, A. N.; Curran, J. S. *J. Chem. Soc., Perkin Trans. 2* **1972**, 2206.

(2) (a) Schlesener, C. J.; Amatore, C.; Kochi, J. K. *J. Am. Chem. Soc.* **1984**, *106*, 7472. (b) Schlesener, C. J.; Amatore, C.; Kochi, J. K. *J. Phys. Chem.* **1986**, *90*, 3747. (c) Masnovi, J. M.; Sankararaman, S.; Kochi, J. K. *J. Am. Chem. Soc.* **1989**, *111*, 2263. (d) Dinnocenzo, J. P.; Banach, T. E. *J. Am. Chem. Soc.* **1989**, *111*, 8646. (e) Reitstöen, B.; Parker, V. D. *J. Am. Chem. Soc.* **1990**, *112*, 4968. (f) Parker, V. D.; Chao, Y.; Reitstöen, B. *J. Am. Chem. Soc.* **1991**, *113*, 2336. (g) Parker, V. D.; Tilset, M. *J. Am. Chem. Soc.* **1991**, *113*, 8778. (h) Xu, W.; Mariano, P. S. *J. Am. Chem. Soc.* **1991**, *113*, 1431. (i) Xu, W.; Zhang, X.; Mariano, P. S. *J. Am. Chem. Soc.* **1991**, *113*, 8863. (j) Zhang, X.; Yeh, S. R.; Hong, S.; Freccero, M.; Albini, A.; Mariano, P. S. *J. Am. Chem. Soc.* **1994**, *116*, 4211. (k) Bacciochi, E.; Del Giacco, T.; Elisei, F. *J. Am. Chem. Soc.* **1993**, *115*, 12290.

(3) (a) Hapiot, P.; Moiroux, J.; Savéant, J.-M. *J. Am. Chem. Soc.* **1990**, *112*, 1337. (b) Anne, A.; Hapiot, P.; Moiroux, J.; Neta, P.; Savéant, J.-M. *J. Phys. Chem.* **1991**, *95*, 2370. (c) Anne, A.; Hapiot, P.; Moiroux, J.; Neta, P.; Savéant, J.-M. *J. Am. Chem. Soc.* **1992**, *114*, 4694.

(4) (a) Fukuzumi, S.; Kondo, Y.; Tanaka, T. *J. Chem. Soc., Perkin Trans. 2* **1984**, 673. (b) Fukuzumi, S.; Tokuda, Y.; Kitano, T.; Okamoto, T.; Otera, J. *J. Am. Chem. Soc.* **1993**, *115*, 8960. (c) Sinha, A.; Bruice, T. C. *J. Am. Chem. Soc.* **1984**, *106*, 7291.

(5) (a) For a review, see the introduction of ref 5b. (b) Anne, A.; Moiroux, J.; Savéant, J.-M. *J. Am. Chem. Soc.* **1993**, *115*, 10224.

(6) (a) For a review, see ref 6b. (b) Savéant, J.-M. *Acc. Chem. Res.* **1993**, *26*, 455.

0002-7863/95/1517-7412$09.00/0 © 1995 American Chemical Society

Chart 1

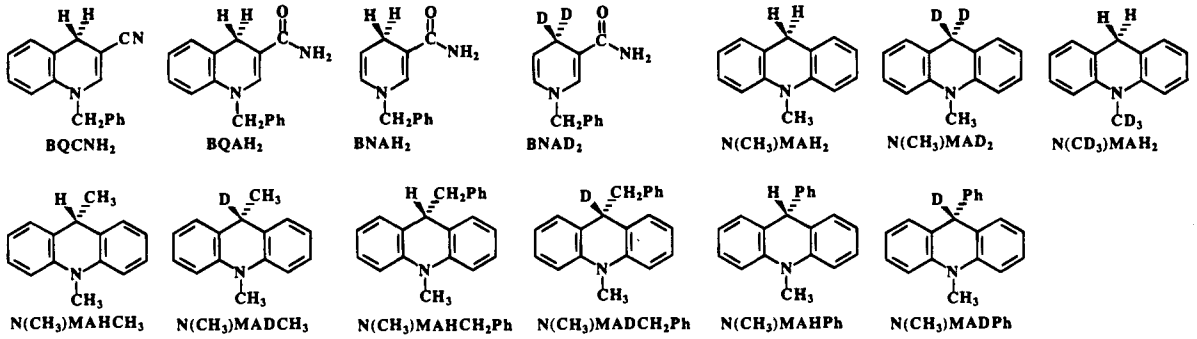

they have been shown to increase with steric hindrance to deprotonation.[8b-e,9]

From the examples investigated so far, evidence for proton tunneling is more elusive for deprotonation of cation radicals although a value of k_H/k_D as high as 22 has been found for the deprotonation of 4-methoxy-*N,N'*-dimethylaniline cation radical by pyridine, against 5 for deprotonation by acetate (values between 5 and 12 were found for 4-Cl, 4-NO_2, and 4-CN substituents).[2g,10] A careful study of the deprotonation of bis-(*p*-anisyl)methylamine cation radical concluded the absence of compelling evidence for tunneling.[2d]

In the methylacridan series, kinetic isotope effects have been previously investigated in the proton transfer that follows the photoinduced electron transfer from benzophenone to $N(CH_3)MAH_2$ producing, in a first stage, the $PhCOPh^{\bullet-}/N(CH_3)MAH_2^{\bullet+}$ radical ion pair.[11] $N(CH_3)MAH_2^{\bullet+}$ and $N(CH_3)MAD_2^{\bullet+}$ were found to deprotonate at the same rate whereas deprotonation was 1.4 times slower for $N(CD_3)MAH_2^{\bullet+}$, indicating[11] that the primary proton transfer involves an hydrogen of the 10-methyl, the ensuing ylid being converted into $N(CHD_2)MAH^{\bullet}$ very rapidly. We included the deprotonation of $N(CD_3)MAH_2^{\bullet+}$ in the present study to see whether this particular behavior is general or is related to the production of the cation radical within a radical ion pair with the anion radical of benzophenone.

(7) With one exception in the methylacridan series,[4b,7b] kinetic isotope effects in NADH analogues so far reported concerned hydride transfer from these molecules[4a,7c,d] rather than deprotonation of their cation radicals.[7e] (b) The determinations of kinetic isotope effect reported in ref 4b as well as the determination of the deprotonation rate constants of the cation radicals and of their pK_a's presented therein will be commented in the Discussion. (c) Yasui, S.; Ohno, A. *Bioorg. Chem.* **1986**, *14*, 70 and references cited therein. (d) He, G. X.; Blasko, A.; Bruice, T. C. *Bioorg. Chem.* **1993**, *21*, 423. (e) Although in one case,[4a] kinetic isotope effects in cation radicals were inferred from kinetic isotope effects in the parent NADH analogues in the framework of an electron–proton transfer mechanism of formal hydride transfer. We will come back to this point in the Discussion.

(8) (a) Melander, L. *Isotope Effects on Reaction Rates*; Ronald Press: New-York, 1960; Chapter 2. (b) Melander, L.; Saunders, W. H. *Reaction Rates of Isotopic Molecules*; Krieger R. E. Publishing Co.: Malabar, FL, 1987; Chapters 2 and 5. (c) Westheimer, F. H. *Chem. Rev.* **1961**, *61*, 265. (d) Bell, R. P. *The Proton in Chemistry*, 2nd ed.; Cornell University Press: Ithaca, NY, 1973; Chapter 12. (e) Lewis, E. S. In *Proton Transfer Reactions*; Caldin, E., Gold, V., Eds.; Chapman and Hall: London, 1975; Chapter 10. (f) Kreevoy, M. M.; Truhlar, D. G. In *Investigations of Rates and Mechanisms of Reactions*; Bernasconi, C. F., Ed.; John Wiley: New York, 1986; Volume 6, Part I, Chapter 1.

(9) (a) Lewis, E. S.; Funderburk, L. H. *J. Am. Chem. Soc.* **1967**, *89*, 2322. (b) Lewis, E. S.; Robinson, J. K. *J. Am. Chem. Soc.* **1968**, *90*, 4337.

(10) (a) The kinetic isotope effect has also been used as a mechanistic tool in the electrochemical oxidation of methylarenes to decide whether deprotonation takes place in the cation radical or in a reversibly formed dimer.[10b] (b) Parker, V. D.; Tilset, M. *J. Am. Chem. Soc.* **1986**, *108*, 6371.

(11) (a) Peters, K. S.; Pang, E.; Rudzki, J. *J. Am. Chem. Soc.* **1982**, *104*, 5535. (b) Mauring, L. E.; Peters, K. S. *J. Am. Chem. Soc.* **1983**, *105*, 5708. (c) Mauring, L. E.; Peters, K. S. *J. Am. Chem. Soc.* **1985**, *107*, 6452.

Scheme 1

$$ARH(D) \rightleftharpoons ARH(D)^{\bullet+} + e^-$$

$$ARH(D)^{\bullet+} + B \xrightarrow{k} AR^{\bullet} + BH(D)^+$$

DISP1: $ARH(D)^{\bullet+} + AR^{\bullet} \xrightarrow{k_{diff}} ARH(D) + AR^+$

ECE: $AR^{\bullet} \longrightarrow ARH(D) + e^-$

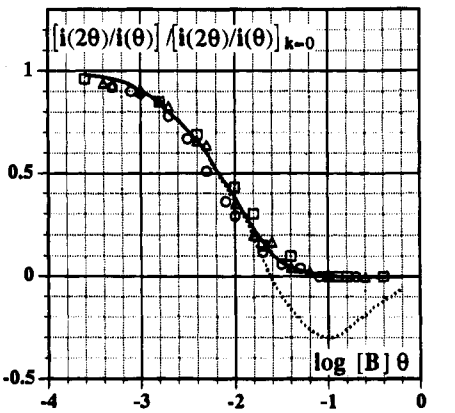

Figure 1. Double potential step chronoamperometric determination of the rate constant of the reaction between 3-chloropyridine (concentration [B] in mM) and $N(CH_3)MAD_2^{\bullet+}$ obtained from oxidation of $N(CH_3)MAD_2$ (5 mM) in acetonitrile and 0.6 M NEt_4BF_4 at a 17 μm diameter gold disk ultramicroelectrode. Temperature: 20 °C. Potential stepping from 0.6 to 1.0 V vs SCE and back. Inversion time: θ (in s). [B] = 50 mM (□), 100 mM (△), and 200 mM (○). The solid line represents the theoretical variation of the current ratio with the dimensionless parameter $\lambda = k[B]\theta$ for a DISP1 mechanism (with $k = 10^{4.4}$ M^{-1} s^{-1}),[12] and the dotted line, the variation of the current ratio for an ECE mechanism with the same parameter λ.[12]

Results

Rate Constants of Proton and Deuteron Transfer. Since the steric and kinetic isotope effects that we are trying to uncover may be small, we cross-checked the data by application of different methods and paid particular attention to reach a reasonable estimate of the uncertainty on each measurement. Particular efforts were also made to cover a large range of driving forces by using a large number of bases. The deprotonation rate constants thus measured fall in the range 10^3 M^{-1} s^{-1} to $10^{9.9}$ M^{-1} s^{-1} (diffusion limit). The highest rate constants were determined by homogeneous redox catalysis (HRC) and laser flash photolysis (LFP), whereas for lower rate constants, we used direct electrochemical methods, double potential step chronoamperometry (DPSC), and cyclic voltammetry (CV) at millimetric or micrometric electrodes.[3] Two difficulties are encountered for low deprotonation rate constants. One is that impurities that are stronger bases than the base under examination, B, may lead to erroneous results even if they are much less concentrated than B. In the determinations described below,

Table 1. Deprotonation Rate Constants and Kinetic Isotope Effects for Cation Radicals of NADH Analogues in the MA and BNA Series (in Acetonitrile at 20 °C)

			log k_H (M^{-1} s^{-1})[c] (log(k_H/k_D)[d])					
			N(CH_3)MARH					
base (B)	p$K_{a\ BH^+}$[a]	method[b]	R = H	R = CH_3	R = $PhCH_2$	R = Ph	N(CD_3)MAH_2	$BNAH_2$
2-chloropyridine(buffered)		DPSCu	4.2[e]					
	6.3	DPSC	4.1 (1.0)				4.1	
		CV	4.1	3.3 (1.0)		3.5 (0.9)		
3-cyanopyridine (buffered)		DPSCu	4.4[e]					
	7.0	DPSC	4.4 (1.1)				4.4	
		CV	4.4	3.4 (0.9)		3.6 (1.0)		
4-chloropyridine (buffered)		DPSCu	4.8[e]					
	8.0	CV	4.7 (0.9)	3.7 (1.0)		3.8 (1.0)	4.7	
		HRC						7.3[h] (0.6)
3-chloropyridine(buffered)		DPSCu	5.1					
	9.0	CV	5.2 (0.8)	3.9 (0.7)		4.2 (0.8)	5.1	
3-fluoropyridine (buffered)		CV	5.3 (0.9)	4.1 (0.8)				
	9.4	CVu	5.2			4.4 (0.8)	5.2	
		HRC						7.8 (0.7)
3-phenylpyridine		CVu	5.7 (0.7)	4.6 (0.4)		5.4 (0.7)	5.6	
	11.6	HRC	5.2					8.5 (0.6)
		CV			4.3 (0.7)			
pyridine	12.3	CVu	6.5 (0.5)	5.2 (0.6)		5.6 (0.5)	6.5	
		HRC	6.5				6.5	8.7 (0.5)
		LFP	6.5	5.5		5.9 (0.6)	6.5	
		CVu	6.3[e] (0.6)	5.3 (0.6)	4.6 (0.5)	5.9 (0.7)	6.4	
3-methylpyridine	13.5	LFP	6.6 (0.6)	5.5 (0.5)	4.7	6.2 (0.7)	6.6	
		HRC						9.0[h] (0.7)
3,5-dimethylpyridine		CVu		5.5 (0.5)	4.6 (0.5)	5.9 (0.4)		
	14.7[f]	HRC	6.9[g] (0.6)				6.7	9.0 (0.7)
		LFP	6.9[g] (0.6)	5.7 (0.4)	4.8	6.3 (0.6)	6.8	
2,5-dimethylpyridine	15.1	CVu			4.6 (0.3)			
		HRC			4.6 (0.3)			8.9 (0.7)
2,6-dimethylpyridine		CVu		4.4 (0.2)	3.4 (0.5)	4.9 (0.5)		
	15.4	HRC	6.9 (0.9)				6.9	8.4 (0.3)
		LFP	6.6 (0.9)	4.7 (0.2)		5.0 (1.0)	6.6	
2,4,6-trimethylpyridine		CVu		5.0 (0.8)	4.0 (0.8)	5.2 (1.0)		
	15.6[f]	HRC	7.4 (0.9)				7.4	8.4 (0.3)
		LFP	7.0 (0.9)	5.1		5.4 (1.3)	7.0	
		CVu			5.7 (0.4)			
benzylamine	16.8	HRC	8.4[g] (0.3)	7.1			8.4	9.3[h] (0.3)
		LFP	8.2	7.0 (0.4)	5.9 (0.3)	7.7 (0.6)	8.2	
tert-butylamine	18.1	HRC	8.6[g] (0.4)	7.4			8.7	9.4 (0.4)
		LFP	8.4[g] (0.4)	7.3 (0.4)	6.2 (0.3)	7.8 (0.2)	8.5	
piperidine	18.9	HRC	9.4[g]					
		LFP		8.0 (0.2)	7.0 (0.2)	8.8 (0.4)	9.2	

[a] p$K_{a\ BH^+}$ in acetonitrile from ref 13 unless otherwise specified. [b] DPSC = double potential step chronoamperometry; CV = cyclic voltammetry; u = ultramicroelectrode; HRC = homogeneous redox catalysis; LFP = laser flash photolysis. [c] Uncertainty = ±0.1. [d] Uncertainty = ±0.2. [e,f,g,h] From refs 3a, 5b, 3b, and 3c, respectively.

this problem was overcome by addition of BH^+ to the solution and verification that the rate constant of deprotonation was independent of BH^+ concentration. A second difficulty derives from the deprotonation of the cation radical by the substrate from which it was produced by oxidation and ensuing decomposition of the protonated substrate. Because of these reactions, a lower limit for reliable determination was 10^3 M^{-1} s^{-1} in the MA series and 10^5 M^{-1} s^{-1} in the BNA series.

Direct Electrochemical Methods. Using the DPSC technique one may check that the oxidation–deprotonation reaction in the MA series follows a DISP1 rather than an ECE mechanism[12] as represented in Scheme 1. The difference in standard potentials of the ARH(D)/ARH(D)$^{\bullet+}$ and AR$^{\bullet}$/AR^+ couples exceeds 1.32 V in all cases (Table 3) pointing to a very large driving force for the DISP1 homogeneous electron-transfer step.

When the deprotonation rate constant is slow, k ≤ $10^{4.5}$ M^{-1} s^{-1}, DPSC and CV may be used with platinum or gold millimetric disk electrodes. One advantage of DPSC over CV is that the potential can be stepped to values negative enough for both ohmic drop and kinetics of initial electron transfer to be negligible. At time θ, the potential is stepped back at a value that can be selected as positive enough for ohmic drop and kinetics of electron transfer to be neglected again. The rate constant is derived from the ratio of the back reduction current (at time 2θ) over the forward oxidation current (at time θ). For convenience, this ratio is normalized toward the value it takes when no follow-up reaction is associated with electron transfer. Observation of the variations with θ and [B] of the ratio $[i(2\theta)/i(\theta)]/[i(2\theta/i(\theta)]_{k=0}$ then allows the determination of the mechanism and of the deprotonation rate constant as illustrated in Figure 1. The use of smaller electrodes ("ultra-microelectrodes" with diameters on the order of 10 μm) results in a decrease of both ohmic drop and cell response time, thus allowing measurements to be made at shorter times in DPSC and higher scan rates in CV and therefore higher deprotonation rate constants to be determined. In the example shown in Figure 1, DPSC was employed with a 17 μm diameter gold disk electrode. It is seen that the variations of the ratio $[i(2\theta)/i(\theta)]/[i(2\theta)/i(\theta)]_{k=0}$

(12) (a) Andrieux, C. P.; Savéant, J.-M. Electrochemical Reactions. In *Investigations of Rates and Mechanisms of Reactions*; Bernasconi, C. F., Ed.; Wiley: New York, 1986; Vol. 6, 4/E, Part 2, pp 305–390. (b) Andrieux, C. P.; Hapiot, P.; Savéant, J.-M. *Chem. Rev.* **1990**, *90*, 723.

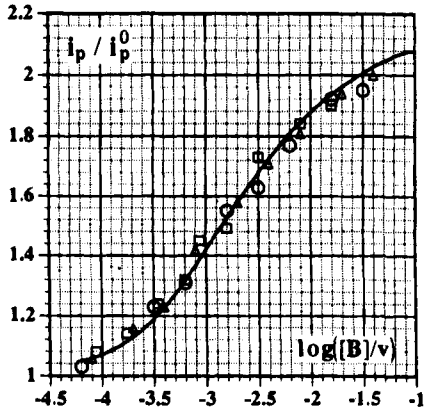

Figure 2. Cyclic voltammetric determination of the rate constant of the reaction between 3-cyanopyridine (concentration [B] in mM) and $N(CD_3)MAH_2^{\bullet+}$ obtained from oxidation of $N(CD_3)MAH_2$ (2.3 mM) in acetonitrile and 0.6 M NEt_4BF_4 at a 1 mm diameter platinum disk electrode. Temperature: 20 °C. Scan rate: v (in V/s). [B] = 17.2 mM (□), 30.9 mM (○), and 39.1 mM (△). The solid line represents the theoretical variation of the current ratio i_p/i_p^0 (i_p, observed peak current, i_p^0, 1e peak current) with the dimensionless parameter $\lambda = RTk[B]/Fv$ for a DISP1 mechanism (with $k = 10^{4.35}$ M^{-1} s^{-1}).[12]

with $[B]\theta$ unambiguously show that the DISP1 mechanism rather than the ECE mechanism is followed. The same conclusion was reached in all cases where the DPSC technique could be used (see Table 1).

CV may be used in a manner similar to that of DPSC, deriving the deprotonation rate constant from the ratio of the cathodic-to-anodic peak current with millimetric as well as with micrometric electrodes. The rate constant may also be derived from the normalized height of the sole anodic peak current since deprotonation of the cation radical makes the electron stoichiometry pass from 1 to 2 electrons per molecule. Variation of the scan rate, v, and/or the concentration of base triggers corresponding variations of the normalized anodic peak current from which the deprotonation rate constant can be extracted as illustrated in Figure 2. For this, the DISP1 rather than the ECE theoretical curve was used for the parameter governing the competition between DISP1 and ECE;[12] $k_{diff}[ARH(D)](Fv/RT)^{1/2}/(k[B])^{3/2}$, has values much in favor of DISP1 in the whole range of deprotonation rates that are accessible by the CV technique (Table 1).

The deprotonation rate constants obtained by means of these two techniques with millimetric or micrometric electrodes are listed in Table 1.

Homogeneous Redox Catalysis. This method was used whenever the deprotonation rate constants were too high to be determined by the two direct electrochemical techniques described above. In the purpose of cross-checking the data, it was also used in a number of cases where the same rate constant is accessible by direct electrochemical techniques (see Table 1). The oxidized form, Q, of a reversible redox couple, P/Q, produced at the electrode surface from P, is used instead of the electrode to generate the cation radical from the substrate. A series of reactions following the initial generation of Q, as shown in Scheme 2, renders the P/Q system irreversible and triggers a catalytic increase of the anodic peak. The ratio of the P-oxidation peaks observed in the presence and absence of the substrate, i_p/i_p^0, is a function of the kinetics of reactions 0, 1, and 2. The mediators we used (*n*-butylferrocene, ferrocene, (4-nitrophenyl)ferrocene, and benzoylferrocene with $E^0_{P/Q}$ values of 0.348, 0.405, 0.523, and 0.655 V vs SCE) were selected so that their standard potentials would be close enough to the oxidation potential of the substrate for obtaining a significant catalytic increase of the peak current but not too close so as to avoid overlapping between the catalytic wave and the direct oxidation wave.

Scheme 2

$$P \rightleftharpoons Q + e^- \qquad (0)$$

$$ARH(D) + Q \underset{k_{-e}}{\overset{k_e}{\rightleftharpoons}} ARH(D)^{\bullet+} + P \qquad (0)$$

$$ARH(D)^{\bullet+} + B \xrightarrow{k} AR^{\bullet} + BH(D)^{+} \qquad (1)$$

$$AR^{\bullet} + Q \xrightarrow{k_{diff}} AR^{+} + P \qquad (2)$$

In all cases, the driving force of reaction 2 is very large, ranging from 0.8 to 1.3 eV (see Table 3). Its rate constant is thus close to the diffusion limit. Since all cation radicals investigated here are strong acids (Table 3), reaction 2 is thus much faster than reverse reaction 1. It follows that forward reaction 1 can be regarded as an irreversible step. i_p/i_p^0 is thus a function of the kinetics of reactions 0 and 1. Two limiting situations may be reached according to the value of the parameter $k_e[P]/k[B]$ that governs the competition between reaction 2 and reverse reaction 1.

When $k_e[P]/k[B]$ is small, reaction 1 is the rate-determining step and no information on the rate constant of interest, k, can be derived from the catalytic current.

Conversely, when $k_e[P]/k[B]$ is large, reaction 1 acts as a pre-equilibrium to reaction 2. $(k_e/k_{-e})k$ can then be derived from the catalytic current using the appropriate working curves. The value of k ensues since $(RT/F)\ \ln(k_e/k_{-e}) = E^0_{P/Q} - E^0_{ARH(D)/ARH(D)^{\bullet+}}$ is known (Table 3). As can be seen from Table 2, describing the homogeneous redox catalysis measurements, this limiting situation was reached only twice in the present study. In all other cases, mixed control by reactions 1 and 2 was encountered. It was still possible to derive k from the catalytic current using another set of working curves[14] even when large values of k made it necessary to lower [B] below the limit where pseudo-first-order conditions are fulfilled.[14c]

For $BNAH_2$ and ferrocene or *n*-butylferrocene, the values of k_e are known from previous work.[3c] Since they are not expected to be affected by deuteriation, the same values were used for $BNAD_2$. Ferrocene, benzoylferrocene and (4-nitrophenyl)-ferrocene were used as mediators with $N(CH_3)MAD_2$ and $N(CD_3)MAH_2$. The values of k_{-e} are already known from previous work.[3c] They were derived from the kinetics of the reaction of ferrocene and benzoylferrocene with $N(CH_3)$-$MAH_2^{\bullet+}$ generated by laser flash photolysis at 308 nm. The values of k_e then result from those of k_{-e} since $E^0_{P/Q}$ and $E^0_{N(CH3)MAH2/N(CH3)MAH2^{\bullet+}}$ are known. Such an approach cannot be employed for (4-nitrophenyl)ferrocene since it absorbs too much in the 308 nm region. The following procedure was thus used in this case. Benzoylferrocene was first used as mediator for determining the deprotonation rate constant of $N(CH_3)$-$MAD_2^{\bullet+}$ by 2,4,6-trimethylpyridine. Then, (4-nitrophenyl)-ferrocene was used with the same substrate and same base. Knowing k for this particular substrate/base system, k_e and k_{-e} were thus found to be 10^4 and $10^{9.8}$ M^{-1} s^{-1}, respectively.

(13) (a) The pK_a's of the pyridinium cations in acetonitrile are from ref 13b; the others are from ref 13c,d. (b) Cauquis, G.; Deronzier, A.; Serve, D.; Vieil, E. *J. Electroanal. Chem. Interfacial Electrochem.* **1975**, *60*, 205. (c) Kolthoff, I. M.; Chantoni, M. K.; Bhownik, S. *J. Am. Chem. Soc.* **1968**, *90*, 23. (d) Coetzee, J. F. *Prog. Phys. Org. Chem.* **1967**, *4*, 76.

(14) (a) Andrieux, C. P.; Blocman, C.; Dumas-Bouchiat; J. M.; M'Halla, F.; Savéant, J.-M. *J. Am. Chem. Soc.* **1980**, *102*, 3806. (b) Andrieux, C. P.; Savéant, J.-M. *J. Electroanal. Chem. Interfacial Electrochem.* **1986**, *205*, 43. (c) Andrieux, C. P.; Anne, A.; Moiroux, J.; Savéant, J.-M. *J. Electroanal. Chem. Interfacial Electrochem.* **1991**, *307*, 17.

Table 2. Homogeneous Redox Catalysis Experiments

base ([B] range in mM)	mediator (P)[a] ([P]/[ARH(D)]in mM/mM)	kinetic control[b]	$N(CH_3)MAD_2$	$N(CH_3)MACH_3H$	$N(CD_3)MAH_2$	$BNAH_2$	$BNAD_2$
4-cyanopyridine							
(25−400)	Fc (2/1)	M					x
3-chloropyridine							
(40−600)	Fc (2/1)	M					x
(10−150)	*n*-Bu-Fc (8/4)	M				x	
3-fluoropyridine							
(2−45)	*n*-Bu-Fc (8/4)	M					x
(3−100)	Fc (2/1)	M					x
3-phenylpyridine							
(2−100)	Fc (2/1)	M					x
(3−110)	*n*-Bu-Fc (8/4)	M				x	x
pyridine							
(5−10) buffered	benzoyl-Fc (2/1)	M			x		
(4−40)	*n*-Bu-Fc (8/4)	M				x	x
3-methylpyridine							
(4−100)	*n*-Bu-Fc (8/4)	M					x
3,5-dimethylpyridine							
(2−100)	*n*-Bu-Fc (8/4)	M				x	
(4−20)	*n*-Bu-Fc (8/4)	M					x
(5−20) (buffered)	benzoyl-Fc (2/1)	1	x		x		
2,5-dimethylpyridine							
(1.5−40)	*n*-Bu-Fc (8/4)	M				x	
(2.6−20)	*n*-Bu-Fc (8/4)	M					x
2,6-dimethylpyridine							
(2−85)	*n*-Bu-Fc (8/4)	M				x	
(2−30)	*n*-Bu-Fc (8/4)	M					x
(5−80)	4-$NO_2C_6H_4$-Fc (2/1)	M	x		x		
2,4,6-trimethylpyridine							
(5−60)	4-$NO_2C_6H_4$-Fc (2/1)	M			x		
(20−80) (buffered)	4-$NO_2C_6H_4$-Fc (2/1)	1	x				
(5−20) (buffered)	benzoyl-Fc (2/1	M	x				
(2−80)	*n*-Bu-Fc (8/4)	M				x	x
benzylamine							
(2−20)	i*n*-Bu-Fc (8/4	M	x		x		x
(3−10)	4-$NO_2C_6H_4$-Fc (2/1))	M					
(10−70)	benzoyl-Fc (2/1)	M		x			
tert-butylamine							
(3−10)	4-$NO_2C_6H_4$-Fc (2/1)	M	x		x		
(2−50)	*n*-Bu-Fc (8/4)	M				x	x
(10−70)	benzoyl-Fc (2/1)	M		x			
piperidine							
(3−10)	Fc (8/4)	M	x				

[a] Fc = ferrocene; *n*-Bu-Fc = *n*-butylferrocene; benzoyl-Fc = benzoylferrocene; *p*-$NO_2C_6H_4$-Fc = (*p*-nitrophenyl)ferrocene. [b] 1 = kinetic control by reaction 1; M = mixed kinetic control by reactions 0 and 1.

Table 3. Determination of the Rate and Equilibrium Constants of Hydride Transfer[a,b]

	N(CH₃)MARH					
	R = CH_3		R = CH_2Ph		R = Ph	
compds	ARH	AR^+	ARH	AR^+	ARH	AR^+
λ_{max} (nm) $10^{-3}\epsilon_{max}$ (M^{-1} cm^{-1})	288	358, 397, 416	286	358, 400, 420	288	358, 400, 420
	35.4	16.4, 2.54, 2.88	20.5	11.13, 4.65, 4.88	12.4	9.95, 4.0, 4.925
λ_{obs} (nm)[c]	397 and 416		400 and 420		400 and 420	
k_3 (M^{-1} min^{-1})	0.007 ± 0.002		0.003 ± 0.0015		0.0035 ± 0.002	
k_{-3} (M^{-1} min^{-1})	0.22 ± 0.01		0.008 ± 0.002		0.028 ± 0.006	
K_3	0.033 ± 0.01		0.45 ± 0.3		0.15 ± 0.1	

[a] In acetonitrile at 20°C. [b] For $BQCNH_2$: λ_{max} = 332 nm, ϵ_{max} = 11 900 M^{-1} cm^{-1}. For $BQCNH^+$: λ_{max} = 330 nm, ϵ_{max} = 14 300 M^{-1} cm^{-1}. [c] Wavelengths at which the kinetic analyses were performed, starting either from AR^+ and $BQCNH_2$ or from ARH and $BQCNH^+$.

Benzoylferrocene was used as mediator with $N(CH_3)MACH_3H^{\bullet+}$. From the variation of k_e with $E^0_{P/Q}$ reported in Table 3 of ref 3c, k_{-e} was estimated as $10^{9.6}$ M^{-1} s^{-1} in this case.

Laser Flash Photolysis. This method[3b,c] was systematically employed in the methylacridan series. The cation radicals were generated by laser flash irradiation at 308 nm of a mixture of the substrate (0.16 mM) and of a dissociative reductive quencher, CCl_4 (10 mM), in aerated acetonitrile. As expected the UV−vis spectra of $N(CH_3)MAH_2^{\bullet+}$, $N(CH_3)MAD_2^{\bullet+}$, and $N(CD_3)MAH_2^{\bullet+}$ are identical (Figure 3). The main absorption peak undergoes a bathochromic shift upon substitution at the 9-position of 10-methylacridan by benzyl and methyl groups and to a lesser extent by phenyl. The other peaks and shoulders present in the UV−vis spectra are also affected by substitution. The λ_{max}'s of the main peak agree with those recently reported[4b] of the same cation radicals generated by reaction of the parents with Fe(III) complexes in the same solvent (recording of the UV−vis spectra was restricted to 600−750 nm and no molar absorbances were given).

An excess of the base, B, or the B/BH^+ buffer, was introduced in the solution ([B] ≥ 100[MARH(D)$^{\bullet+}$]). As illustrated in Figure 4, the deprotonation (dedeuteronation) rate constant was

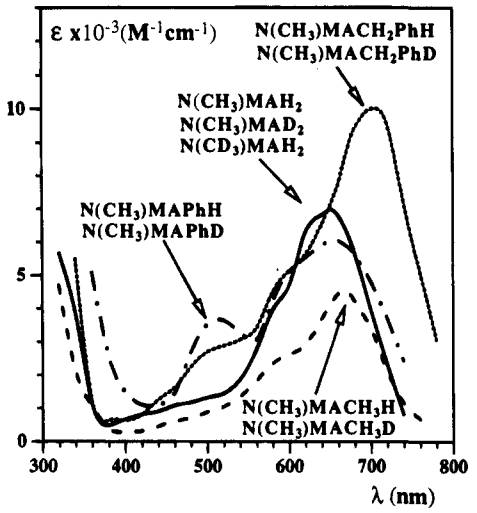

Figure 3. UV−vis absorption spectra of cation radicals in the methylacridan series (recorded 1 μs after the pulse).

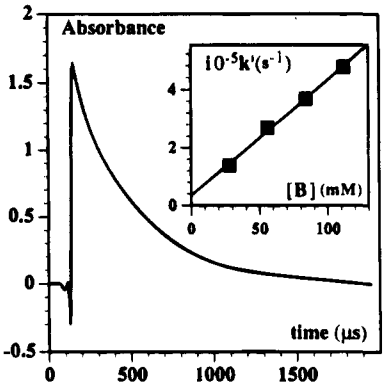

Figure 4. Decay of the absorbance of $N(CD_3)MAD_2^{\bullet+}$ generated by LFP of $N(CD_3)MAD_2$ (0.16 mM) in acetonitrile, 0.1 M NEt_4BF_4, 10 mM CCl_4, 56 mM 2,6-dimethylpyridine, and 23 mM $HClO_4$. Temperature: 21 ± 1 °C. Irradiation by a 10−20 ns, 80−150 mJ laser pulse at 308 nm. The insert reproduces the plot of the rate constant k' of the observed pseudo-first-order kinetics vs the 2,6-dimethylpyridine concentration [B].

then obtained from the decay in absorbance of the cation radical, at 640 nm for $N(CH_3)MAH_2^{\bullet+}$, $N(CH_3)MAD_2^{\bullet+}$, $N(CD_3)MAH_2^{\bullet+}$, $N(CH_3)MAPhH^{\bullet+}$, and $N(CH_3)MAPhD^{\bullet+}$ and at 670 nm for $N(CH_3)MACH_3H^{\bullet+}$, $N(CH_3)MAPhD^{\bullet+}$, $N(CH_3)MACH_2PhH^{\bullet+}$ and $N(CH_3)MACH_2PhD^{\bullet+}$. The global rate constant, k', was observed to obey pseudo-first order kinetics, and the final second-order rate constant was derived from the slope of the first-order rate constant vs [B] plot as illustrated in the insert of Figure 4. Addition of *t*-$BuNBF_4$, the supporting electrolyte used in the electrochemical experiments, had no effect on the k values thus determined. The values of k_H and k_D thus obtained are listed in Table 1.

Determination of Thermodynamic Parameters. The pK_a's of the cation radicals are needed to correlate the deprotonation rate constants with the driving force expressed as the difference of these pK_a's with the pK_a's of the opposing bases. The pK_a's of the cation radicals were derived from the following equation:

$$\left(\frac{RT}{F}\ln 10\right)pK_{a\ ARH^{\bullet+}} = 2E^0_{ARH/AR^+} - E^0_{ARH/ARH^{\bullet+}} + E^0_{AR^{\bullet}/AR^+}$$

where the various standard potentials were determined as follows.

$E^0_{ARH/ARH^{\bullet+}}$'s were obtained from cyclic voltammetry of the substrates, at millimetric or micrometric electrodes, in the presence of the weakest opposing bases so that reversibility could be reached without difficulty.

The $E^0_{AR^{\bullet}/AR^+}$'s were obtained by reductive cyclic voltammetry of the AR^+ cations. The corresponding reduction wave is irreversible at low scan rates owing to dimerization of the $AR^{\bullet}$ radical resulting from the reduction of AR^+ :

$$AR^+ + e^- \rightleftharpoons AR^{\bullet} \qquad 2\,AR^{\bullet} \rightarrow RA{-}AR$$

With $BNAH^+$, $N(CH_3)MAH^+$, and $N(CH_3)MACH_3^+$, the dimerization is fast ($\approx 10^8\ M^{-1}\ s^{-1}$) and ultramicroelectrodes and high scan rates are required to reach reversibility and thus measure the standard potential. This is not the case with $N(CH_3)MAPh^+$ and $N(CH_3)MACH_2Ph^+$ where reversibility is met at only 1 V/s.

To obtain the E^0_{ARH/AR^+}'s, we determined, by UV−vis spectrometry, the forward and reverse rates, and thus the equilibrium constant, of hydride transfer between the substrate of interest and another NADH analogue whose E^0_{ARH/AR^+} is already known according to a previously described procedure.[15] The E^0_{ARH/AR^+} of the reference NADH analogue should not be too different from the NADH analogue of interest for the rate constants in both directions to be accessible within a reasonable amount of time. $BQCNH_2$ was found to fulfill this requirement and was thus selected as reference compound to be reacted with the compound of interest as represented in the following equation:

$$AR^+ + BQCNH_2 \underset{k_{-3}}{\overset{k_3}{\rightleftharpoons}} BQCNH^+ + ARH$$

The spectroscopic characteristics of the ARH and AR^+ species and the wavelengths at which the absorbances were monitored are reported in Table 3. Then

$$E^0_{ARH/AR^+}\ (\text{in V vs SCE}) = E^0_{BQCNH_2/BQCNH^+}\ (0.257 \pm 0.026) + 0.029 \log K_3$$

The resulting values of E^0_{ARH/AR^+} are listed in Table 4 which also contains the ensuing values of the cation radical pK_a's. We have also determined, according to the same procedure as already described,[3c] the homolytic bond dissociation energies of cation radicals ($\rightarrow AR^+ + H^{\bullet}$), another thermodynamic parameter of interest for the following discussions. These various thermodynamic parameters are gathered in Table 4.

The main uncertainty on pK_a's comes from the E^0_{ARH/AR^+}'s. In the cascade determination of the latter parameter, the main part of the uncertainty originates from hydride-transfer equilibration between $N(CH_3)MAH_2$ and 1,4-naphthoquinone.[3a] In terms of relative pK_a's, the uncertainties are less: if we take the value for $N(CH_3)MAH_2$ as reference, the uncertainties on the other pK_a's are only 0.2−0.3 units.

Discussion

The variations of the deprotonation rate constant with the driving force, as measured by the difference between the pK_a of the opposing base and the pK_a of the cation radical, are represented in Figure 5 for the various cation radicals investigated in this work. It clearly appears that these systems are under activation control in most of the driving force range with average symmetry factors around 0.35−0.40.

The cation radicals of substituted methylacridans are strong acids, as is the cation radical of methylacridan itself, having pK_a's (in acetonitrile) ranging from 0.8 to 1.7 (Table 4). This

(15) Anne, A.; Moiroux, J. *J. Org. Chem.* **1990**, *55*, 4608.

Table 4. Thermodynamic Parameters for the Deprotonation of NADH Analogues Cation Radicals

	N(CH$_3$)MARH				
compds	R = H[b]	R = CH$_3$	R = CH$_2$Ph	R = Ph	BNAH$_2$[c]
$E^0_{ARH/ARH^{\bullet+}}$[a]	860 ± 4	885 ± 4	890 ± 4	935 ± 4	785 ± 8
$E^0_{AR^{\bullet}/AR^+}$[a]	−465 ± 10	−540 ± 10	−505 ±4	−545 ± 6	−1105 ± 10
E^0_{ARH/AR^+}[a]	220 ± 24	213 ± 30	243 ± 36	229 ± 36	−22 ± 39
$pK_{a\ ARH^{\bullet+}}$	0.8 ± 1.1	1.5 ± 1.3	1.7 ± 1.4	1.2 ± 1.4	4.7 ± 1.3
$D_{ARH^{\bullet+}/AR^+ + H^{\bullet}}$ (eV)	1.80 ± 0.07	1.77 ± 0.09	1.81 ± 0.09	1.74 ± 0.09	1.39 ± 0.09

[a] In mV vs SCE. [b] From refs 3a,c. [c] From refs 3c and 15.

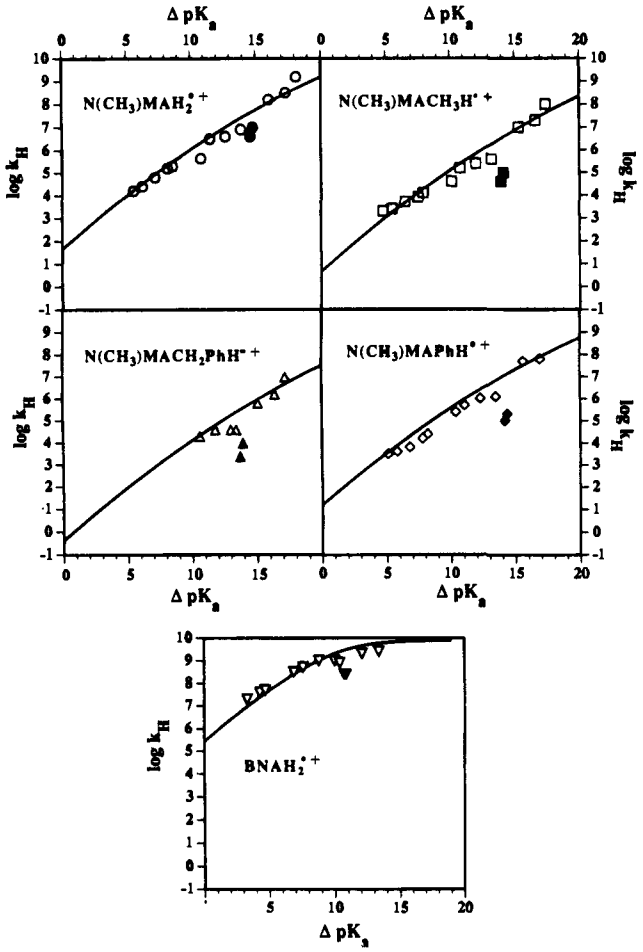

Figure 5. Variation of the deprotonation rate constant of the cation radicals with the driving force.

conclusion is not shared by another group working in the field which reports values as high as 8 for the pK_a of N(CH$_3$)MAH$_2^{\bullet+}$ and N(CH$_3$)MACH$_3$H$^{\bullet+}$.[4b,16a] Although the thermodynamic analysis that led to our values suffers no ambiguity, it is worth examining the origin of these discrepancies.

In an earlier work, the same group derived the pK_a of N(CH$_3$)MAH$_2^{\bullet+}$ in acetonitrile from the variation of the deprotonation rate constant with the pK_a of a series of opposing bases,[16b] i.e., from the same type of plots as those shown in Figure 5. However, instead of plotting log k against the pK_a's of the bases in acetonitrile, it was plotted against the pK_a's of the bases in water. The ensuing narrowing of the pH scale then resulted in a higher slope unduly indicating that the deprotonation was not under activation control but rather that the reverse (protonation) reaction was under diffusion control. The pK_a of the cation radical was then derived from the intersection of the log k straight line with an erroneous slope with an horizontal representing diffusion control. An additional source of error was that the latter was actually taken 3.5 below the diffusion limit. The ensuing pK_a of the cation radical, 2 in the water pH scale, even translated to a value of 8.5 in the acetonitrile pH scale, is therefore meaningless. The log k—pK_a (in acetonitrile) slopes found here (Figure 5) as well as those in ref 16b unambiguously demonstrate that the deprotonation reaction is under activation control.

(16) (a) Fukuzumi, S.; Tokuda, Y. *Chem. Lett.* **1992**, 1721. (b) Fukuzumi, S.; Kumitsu, S.; Hironaka, K.; Tanaka, T. *J. Am. Chem. Soc.* **1987**, *109*, 305.

Scheme 3

$$ARH + Ox \longrightarrow ARH^{\bullet+} + Red \qquad (0')$$

$$ARH^{\bullet+} (+ H_2O) \underset{k_p}{\overset{k_d}{\rightleftharpoons}} AR^{\bullet} + H^+(H_3O^+) \qquad (1')$$

$$AR^{\bullet} + Ox \xrightarrow{k_{et}} AR^+ + P \qquad (2')$$

Another strategy has been employed more recently.[4b,16a] The cation radical is generated in acetonitrile by stopped-flow oxidation of the substrate with Fe(ClO$_4$)$_3$, [Fe(phen)$_3$]$^{3+}$, or Cu(ClO$_4$)$_2$ (Ox). After the flow is stopped, the decay of the cation radical, monitored by UV—vis spectrometry, exhibits second-order kinetics in an early stage and then first-order kinetics. The latter were rationalized according to Scheme 3 in which reaction 0′ is regarded as irreversible from left to right and the cation radical is assumed to deprotonate spontaneously. The experiments were conducted in the presence of perchloric acid, and the k vs [Ox] data were thus analyzed according to the following equation:

$$\frac{1}{k_{1'}} = \frac{1}{k_d} + \frac{k_p}{k_d k_{et}} \frac{[H^+]}{[Ox]}$$

(Figure 6 in ref 4b, Figure 2 in ref 16a) leading to a straight line for each value of [ClO$_4$H] whose intercept provides k_d while the slope gives k_p/k_d and therefore the pK_a of the cation radical. It was thus found that both k_d and the pK_a depended on the concentration of perchloric acid. This surprizing observation was explained by invoking a possible role of water which is unavoidably introduced together with ClO$_4$H (added as a 70% aqueous solution). Water may indeed acts as a base (pK_a 2.3—2.7 in acetonitrile[13d]) deprotonating the cation radical as represented between parentheses in Scheme 3. If we pursue the analysis of the rate data along those lines, we have to use the following equation instead of the previous one:

$$\frac{1}{k_{1'}} = \frac{1}{k_d^*[H_2O]} + \frac{k_p}{k_d^* k_{et}} \frac{[H_3O^+]}{[H_2O][Ox]} = \frac{1}{k_d^*([H_2O]_r + 2.4[ClO_4H])} + \frac{k_p}{k_d^* k_{et}} \frac{[H_3O^+]}{([H_2O]_r + 2.4[ClO_4H])[Ox]}$$

k_d^* is the second-order rate constant of deprotonation of the cation

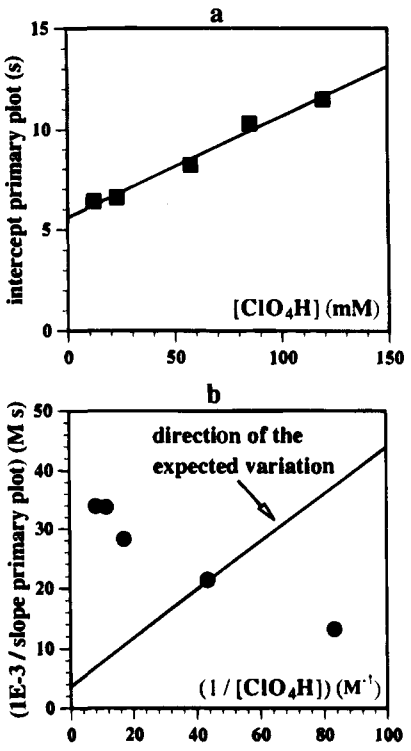

Figure 6. Analysis of the rate data of ref 4b and 17a.

radical by water, $[H_2O]_r$ is the residual concentration of water prior to addition of ClO_4H, while the factor 2.4 stands for the number of moles of water introduced per mole of ClO_4H. We may then plot $k_d = k_d^*[H_2O]$ against $[ClO_4H]$ as shown in Figure 6a. From the intercept and slope of the straight line thus obtained, one obtains k_d^* 20.8 M^{-1} s^{-1} and $[H_2O]_r$ = 0.27 M. We may also examine how the apparent pK_a derived from the slope of the primary plot varies with $[ClO_4H]$. This slope is expected to obey the following relationship:

$$\frac{1}{\text{slope}} = \frac{k_d^* k_{et}}{k_p}\left(2.4 + 0.27\frac{1}{[ClO_4H]}\right)$$

Figure 6b shows that the experimental data do not follow these expectations. There is more than a quantitative disagreement since the experimental and predicted variations are opposite in sign. In other words, the slope of the primary plot should increase toward a constant value as $[ClO_4H]$ increases whereas it actually decreases toward a constant value as $[ClO_4H]$ increases. We can thus conclude that the observed kinetics are inconsistent with the reaction scheme assumed for deriving the pK_a of the cation radical, thus leading to an apparent value that is not related to the actual pK_a. In fact, the cation radical is so strong an acid that forward reaction 1′ is the rate-determining step. That this is indeed the case appears in the results of direct electrochemical oxidation as illustrated in Figures 1 and 2. If a DISP2 mechanism (where in Scheme 1 reaction 1 would have acted as a pre-equilibrium to reaction 2) were followed, the data points would not fit the DISP1 curve.[12] From Figure 5, it is predicted that, with water, k_p should be on the order of 20 M^{-1} s^{-1} and should therefore be unable to compete with k_{et}, which is certainly close to the diffusion limit in view of the large driving force of reaction 2′ as well as reaction 2 (as seen in Table 3, the standard potential for the reduction of AR^+ is −0.465 V vs SCE). The observed variations of the kinetics with the concentration of the oxidant are in fact more likely to result from the effect on k_d of the water that is introduced together with the oxidant (9 mol of water for 1 mol of $FeClO_4$). The rate data are indeed reproduced correctly in this framework although with some scatter of the experimental points around the predicted curves. In this connection, there is a second source of concern in the manner in which the rate data were processed in ref 4b and 16a. The second-order kinetics observed in the early stage of the cation radical decay were interpreted as a consequence of the disproportionation reaction:

$$2\,ARH^{\bullet+} \rightarrow AR^+ + ARH + H^+$$

which implies that

$$ARH^{\bullet+} + AR^{\bullet} \rightarrow AR^+ + ARH \qquad (2'')$$

replaces reaction 2′ in Scheme 3, the latter reaction being also diffusion controlled since it has a very large driving force (1.33 eV). For the same reasons as developed above in the case of reaction 2′, reaction 2″ should not interfere in the observed second-order kinetics. These are more likely related to the fact that the AH substrate is not completely consumed in the early stages of the cation radical decay as results from previous determinations of the rate constant for the oxidation of $N(CH_3)$-MAH_2 by $Fe(ClO_4)_3$[17] (0.2−0.5 s half-decay time for $Fe(ClO_4)_3$ concentrations ranging from 5 to 0.5 mM). It may therefore serve as a base (pK_a = 3.3)[15] competing with water in the deprotonation of the anion radical. The ensuing overlap of the reaction of the cation radical with the parent substrate and the reaction with water may well affect the accuracy of the kinetic data pertaining to the deprotonation by water. In the present study, only bases that are significantly stronger than either water or the substrate ($pK_a \geq 6$) were used for avoiding such complications. We can thus conclude that these experimental observations can be rationalized in the framework of the pK_a values determined in the present work from thermodynamical cycles.

Steric hindrance to deprotonation appears in two ways in the activation/driving force plots in Figure 5. First, the two pyridines bearing methyl groups in both the 2 and 6 positions give rise to data points that fall significantly below the log $k-\Delta pK_a$ best-fit parabolas pertaining to the unencumbered bases. The effect is modest with $N(CH_3)MAH_2^{\bullet+}$ and $BNAH_2^{\bullet+}$ (~60 meV in terms of energy) but larger with the C-alkylated cation radicals (~120 meV). With only one methyl group in the 2 position, the steric effect is negligible (Table 1). Introduction of an alkyl or aryl group at the functional carbon also results in a decrease in reactivity. This effect is best seen in a plot of the intrinsic barrier free energies (derived from the intercepts of the best-fit parabolas in Figure 5) versus the bond dissociation energies of the cation radicals ($ARH^{\bullet+} \rightarrow AR^+ + H^{\bullet}$, see Table 4) as represented in Figure 7. As discussed earlier, in the absence of encumbering alkyl groups, there is a correlation between these two quantities pointing to the concept that their deprotonation may be viewed as a concerted H-atom/electron transfer.[3c] It is seen (Figure 7) that the points representing the C-alkylated cation radicals fall above the line, pointing to significant steric hindrance to deprotonation. However the effect is again modest (70, 90 and 100 meV). The kinetic isotope effects are represented in Figure 8 under the form of plots of $\log(k_H/k_D)$ against the driving force, ΔpK_a. The very existence of distinct kinetic isotope effects (KIE) provides confirmation of the assignment of deprotonation of the cation radical as the rate-determining step in the direct and redox-catalyzed oxidation of the various substrates. We also note that the deprotonation rate constants of $N(CH_3)MAH_2^{\bullet+}$ and $N(CD_3)MAH_2^{\bullet+}$ are the same over the whole series of bases (Table 1). This observation

(17) Fukuzumi, S.; Mochizuki, S.; Tanaka, T. *J. Chem. Soc., Dalton Trans.* **1990**, 695.

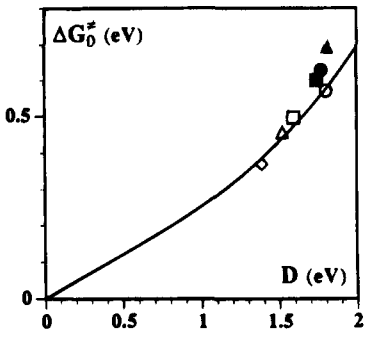

Figure 7. Plot of the intrinsic barrier free energies against the bond dissociation energies: ◇, $BNAH_2^{\bullet+}$; △, $BQAH_2^{\bullet+}$; □, $BQCNH_2^{\bullet+}$; ○, $N(CH_3)MAH_2^{\bullet+}$; ■, $N(CH_3)MAPhH^{\bullet+}$; ●, $N(CH_3)MACH_3H^{\bullet+}$; ▲, $N(CH_3)MACH_2PhH^{\bullet+}$.

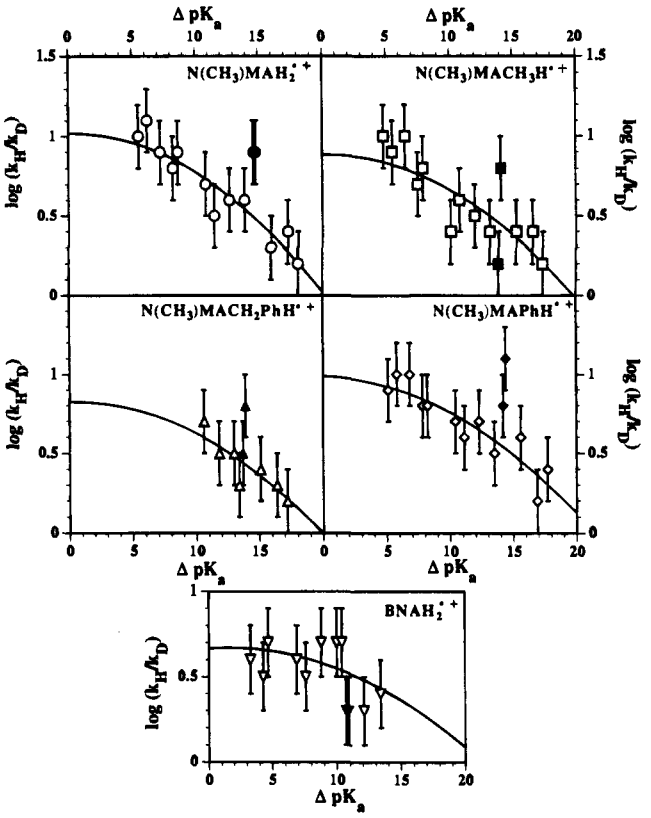

Figure 8. Kinetic isotope effect as a function of the driving force. Solid symbols represent the 2,6-dimethylpyridines.

shows that the protons borne by the methyl group linked to the nitrogen atom in methyl acridan are not involved in the deprotonation of the cation radicals. It thus appears that the involvement of a methyl proton in the case where the cation radical was produced by photoinduced electron transfer from benzophenone is related to its production within a radical ion pair.[11]

Overall, the magnitude of these effects is small, k_H/k_D ranging from 2 to 12 as a function of the substrate and of the basicity of the opposing base. There is a small but distinct tendency for the KIE to decrease upon increasing the driving force. It appears more clearly in the methylacridan series than with $BNAH_2^{\bullet+}$. At zero driving force, the KIE is slightly larger in the methylacridan series (k_H/k_D = 8.4 in average) than with $BNAH_2^{\bullet+}$ (k_H/k_D = 5.6). Perusal of the diagrams in Figure 8 shows that the increase of steric hindrance due to encumbering of bases or of the functional carbon of the cation radical or both does not results in any significant increase of the KIE. This observation and the rather low values of the KIE point to the conclusion that there is no compelling evidence that proton (or H-atom) tunneling plays a major role in the deprotonation of the cation radicals. The observed variation of the KIE from acridans to $BNAH_2$ rather derives from changes in zero-point energies in the cation radicals, and the variation with the driving force may be related to variation of the symmetry factor as discussed earlier.[8b,d]

Conclusions

In summary, all the cation radicals in the methylacridan series are strong acids, with pK_a's ranging from 0.8 to 1.7, as results from thermodynamic cycles involving measured standard potentials and hydride-transfer equilibrium constants. Significant steric hindrance to deprotonation results from encumbering of the opposing base and of the functional carbon in the cation radical. Kinetic isotope effects, ranging from 2 to 12 in terms of k_H/k_D, appear upon substituting H to D at the functional carbon of the cation radical. This observation confirms the assignment of deprotonation of the cation radical as the rate-determining step in the direct and redox-catalyzed oxidation of the various NADH analogues investigated in this study. The absence of isotope effect upon substitution of the *N*-methyl group in the methylacridan series shows that these protons are not involved in the deprotonation reaction. The very fact that the observed kinetic isotope effects are small and the fact that they do not increase with steric hindrance show that proton (or H-atom) tunneling does not interfere to any significant extent in the deprotonation reaction.

Experimental Section

Chemicals. $N(CH_3)MAH_2$, $N(CH_3)MAD_2$, $N(CD_3)MAH_2$, and $BNAH_2$, and $BNAD_2$ were prepared according to procedures described in ref 18, 19, 18, 20, and 21, respectively, through multistep synthetic routes. The corresponding AH^+ cations were obtained and could be isolated at one stage of these processes. $N(CH_3)MACH_3H$, $N(CH_3)MACH_2PhH$, and $N(CH_3)MAPhH$ were obtained by addition of the corresponding Grignard reagent RMgI (or Br) to 10-methylacridinium. Typically, 4.2 mL of a 3 M solution of RMgX in diethyl ether was added to a suspension of 10-methylacridinium (10 mmol in 10 mL of the same solvent). After *ca.* 20 min, the mixture was hydrolyzed with 30 mL of an aqueous 20% NH_4Cl solution. Once filtrated, the resulting precipitate was extracted with ether. After neutralization of the organic phase by repeated aqueous washings, ether was evaporated under vacuum. The pure final product was then obtained by recrystallization of the solid from ethanol/water. Final yield: 70−80%. The AR^+ compounds were prepared as follows: *p*-Chloranil (0.16 mmol) was dissolved in acetonitrile (4 mL) under nitrogen atmosphere and ultrasonication; solid ARH (0.15 mmol) was then added. After *ca.* 30 min, the mixture was acidified with 0.4 mL of 1 M aqueous HCl and filtrated and the solvent was evaporated. A solution of the residue in water (10 mL) was extracted with CH_2Cl_2. Evaporation of the aqueous phase to dryness gave the salt which was recrystallized from ethanol/water. Final yield: *ca.* 80%. Each of the deuteriated ARD substrates was obtained through overnight reduction in ether under reflux by an excess of $LiAlD_4$ (10 times). The precipitate resulting from the hydrolysis by D_2O in excess (100 times) was extracted with ether. Evaporation of the solvent of the organic phase and recrystallization

(18) Roberts, R. M. G.; Ostovic, D.; Kreevoy, M. M. *Faraday Discuss. Chem. Soc.* **1982**, *74*, 257.

(19) (a) Karrer, P.; Szabo, L.; Krishna, H. V. J.; Schwyzer, R. *Helv. Chim. Acta* **1950**, *33*, 294. (b) Ostrovic, D.; Roberts, R. M. G.; Kreevoy, M. M. *J. Am. Chem. Soc.* **1983**, *105*, 7629.

(20) (a) Mauzerall, D.; Westheimer, F. H. *J. Am. Chem. Soc.* **1955**, *77*, 2261. (b) Anderson, A. G.; Berkelhammer, G *J. Am. Chem. Soc.* **1958**, *80*, 992.

(21) (a) Braude, E. A.; Hannah, J.; Linstead, R. *J. Chem. Soc.* **1960**, 3249. (b) Caughey, W. S.; Schellenberg, K. A. *J. Org. Chem.* **1966**, *31*, 1978. (c) Fukuzumi, S.; Nishizawa, N.; Tanaka, T. *J. Org. Chem.* **1984**, *49*, 3571 and ref 3.

of the remaining solid from ethanol/water gave ARD with a 60−70% yield. The identification and the purity of all products were confirmed by chemical, mass, and ^{1}H NMR spectrometric analyses.

Instrumentation and Procedures. The procedures and instrumentation, except for LFP, were the same as previously described.[1,13] For the LFP experiments, a Questek 2320 excimer laser operated at 308 nm (XeCl) was used to irradiate a 1.8 cm long, 0.8 cm high rectangle located at the center of one side of the reaction cell which was 2 cm long, 1 cm high, and 0.5 cm thick. The laser produced pulses of 100−200 mJ energy and 20−40 ns duration. The cell was filled with a new solution before each pulse. For kinetic spectrophotometric detection, the light from a 150 W xenon arc lamp was focused through the cell (perpendicularly to the irradiation beam and to the 0.5 × 1 cm side of the cell) into the entrance slit of a Jobin Yvon H20 monochromator. The changes in absorbance at a given wavelength were monitored by a Hamamatsu R446 photomultiplyer connected to a Nicolet 360 digital oscilloscope. Data were transfered to a PC 486DX50 microcomputer for treatment and least-square analysis. The molar absorbances of the cation radicals $ARH^{+\cdot}$ were determined as follows. At long times, each transient $ARH^{+\cdot}$ species was finally transformed into a AR^+ species whose absorption spectrum is well-known. There existed always wavelength intervals in which AR^+ was the only component of the reaction mixture to absorb appreciably. Hence, its concentration $C_{AR}{}^+$, typically in the 0.01−0.05 mM range, could be evaluated easily. At any wavelength at which $ARH^{+\cdot}$ was the only species to absorb at very short times, its molar absorbance was then readily deduced from the measured absorbance by assuming that its concentration was $C_{AR}{}^+$.

JA950658Q